NJC

Accepted Manuscript

This article can be cited before page numbers have been issued, to do this please use: R. Rani, G. Sharma, K. D. Paul and V. Luxami, *New J. Chem.*, 2018, DOI: 10.1039/C8NJ00741A.

ROYAL SOCIETY OF CHEMISTRY

rsc.li/njc

View Article Online
DOI: 10.1039/C8NJ00741A

Journal Name

ARTICLE

Donor-π-Acceptor (D-π-A) Dyad for ratiometric detection of Hg^{2+} and PPi

[1]Received 00th January 20xx,
Accepted 00th January 20xx

DOI: 10.1039/x0xx00000x

www.rsc.org/

Richa Rani[#], Gulshan Kumar[#], Kamaldeep Paul, and Vijay Luxami*

A donor-π-acceptor (D-π-A) dyad **1** has been successfully synthesized by linking phenanthrenequinone as an electron donor unit and anthraquinone as an electron acceptor unit through a phenyl ring. Dyad **1** exhibits the intramolecular charge transfer and acts as a key phenomenon for the detection of Hg^{2+} and of pyrophosphate ion ($P_2O_7^{4-}$, PPi) in the semi-aqueous medium. The dyad **1** exhibits absorption peaks at 430, 370, and 337 nm and an emission peak at 530 nm (λ_{ex} = 430 nm). Dyad **1** exhibits new absorption peak at 390 nm ratiometrically along with emission quenching in the presence of Hg^{2+} ions while the presence of PPi results in drastic ratiometric changes in absorption and emission spectra with a new peak at 495 nm and 620 nm, respectively. The quantum yield of the dyad **1** on complexation with PPi has also been increased from 0.1 (free dyad) to 0.69 (dyad **1**.PPi). The lowest detection limits for Hg^{2+} and PPi found to be 31 nM and 46.5 nM, respectively. DFT calculations have been performed to develop the mode of a mechanism for PPi and Hg^{2+} ions binding with dyad **1**.

1. Introduction

The luminescent molecules are giving the impression as an ideal candidate for applications in biology, environment, and chemical sensing due to high selectivity, sensitivity, fast analysis, easy sample preparation, and providing real-time information.[1-3] Fluorophore like BODIPY, rhodamine, and fluorescein are being used in various biological and environmental applications. Numerous approaches have been employed in literature to increase the sensitivity and selectivity in chemical sensing, including internal charge transfer (ICT), fluorescence enhancement, fluorescent quenching, Förster resonance energy transfer (FRET), excited state proton transfer (ESPT), photoinduced electron transfer (PET) etc.[4-8] Among these approaches, ICT is a powerful phenomenon in developing fluorescent molecules, consisting of an electron donor (D) and an electron acceptor (A) which further provides sensible resolution for chemical sensing, and covers the visible light region from blue to red colour. Donor-acceptor based conjugated molecular systems are very sensitive to their local environment and thus widely used in other applications such as optoelectronic device, diagnostic and optical imaging. In general, upon absorption of a photon, donor- π -acceptor (D-π-A) molecular system gets excited to their local excited state, which further undergoes charge separation in an excited state at their donor and acceptor units. The charge-separated excited state was stabilized by the local environment that resulted in drastic changes in optical properties. The intramolecular charge transfer can be modulated by (i) geometrical symmetry and constraints, (ii) the energy gap between the frontier molecular orbitals and (iii) using a connector between donor and acceptor.[9-12] Apparently, the intramolecular charge transfer molecular systems exhibit significant emission changes by altering the excited state.

The mercury pollution is extensive among various heavy metal ions with toxicological profile to human and environment. The presence of mercury in batteries, paints, and other electronic goods etc. (which are materials of our daily life) increase the human health and environment concerns. Considering these concerns, efforts have been made for recognition and quantification of Hg^{2+} ions in environmental samples through developing various chromo-fluorescent chemosensors. These chemosensors were found to be potential candidate due to high selectivity, sensitivity, real time analysis.[13-19] Therefore, we here reporting dyad 1 based on ICT phenomenon, which could potentially detect the mercury and PPi.

The dyad 1 contains 1*H*-phenanthro[9,10-*d*]imidazole as an electron rich, also known for electron donor candidate, while the anthraquinone is known to be an electron acceptor candidate due to the presence of two carbonyl groups as electron withdrawing units.[20-22] Both the 1*H*-phenanthro[9,10-*d*]imidazole and anthraquinone units are used to modulate the intramolecular charge transfer separately and have been used as material with application in dyes, chemical sensing,

School of Chemistry and Biochemistry, Thapar Institute of Engineering and Technology, Patiala-147004, India.
E-mail: vluxami@thapar.edu
†Electronic Supplementary Information (ESI) available: [^{1}H NMR , ^{13}C NMR, MS, Job plot, calibration curve for lowest detection limit, ref for Gaussian]. See DOI: 10.1039/x0xx00000x
# Both authors have equal contribution

View Article Online
DOI: 10.1039/C8NJ00741A

pharmaceutics and biology.[23-30] According to the best of our knowledge, the combination of 1*H*-phenanthro[9,10-*d*]imidazole and anthraquinone has not been explored for chemical sensing. In the present manuscript, we have employed intramolecular charge transfer strategy to develop donor-π-acceptor (D-π-A) based dyad **1** by linking 2-phenyl-1*H*-phenanthro[9,10-*d*]imidazole as a donor moiety with 3*H*-anthra[1,2-*d*]imidazole-6,11-dione as an acceptor moiety through phenyl ring as a π-conjugated system. The developed D-π-A system of dyad **1** showed absorption peaks at 430, 370, and 337 nm and an emission peak at 530 nm (λ_{ex} = 430 nm). Dyad **1** showed an absorption ratiometric response for Hg^{2+} with the emergence of a new band at 390 nm along with emission quenching. However, the presence of pyrophosphate ions (PPi) in dyad **1** resulted in new absorption band at 495 nm and emission band at 620 nm ratiometrically in the semi-aqueous medium. In literature, there are reports for PPi detection through metal chelation, where the sensor molecules were first chelate to metal ions and the following complex were used for PPi detection.[31-44] There are very few reports, where the sensor molecule directly interact to PPi. In continuation to our previous efforts of PPi detection, here, we are reporting D-π-A based molecular sensor (dyad **1**) which successfully detect PPi without metal template support. Thus, this report overcomes the limits of metal chelation in the previous reports. The density functional theory (DFT) calculations were also endorsing the experimental results. It has been found that the PPi interacted to dyad **1** through hydrogen bonding, which was further studied through atoms in molecule (AIM) approach.

2. Experimental section

2.1. Materials and methods

All the chemicals used for synthesis were purchased from Sigma-Aldrich Chemical Ltd., and Loba Chemie depending upon their availability. All the solvents used were of spectroscopic grade purchased from Spectrochem and Rankem Ltd. All chemicals and solvents were used without any further purification. The progress of the chemical reaction was monitored by means of thin-layer chromatography (TLC). Melting points were recorded in open capillary tube and were uncorrected. ^{1}H NMR and ^{13}C NMR spectra were recorded on JEOL ECS-400 MHz spectrometer at ambient temperature in $CDCl_3$ or/and DMSO-d_6 with TMS as an internal reference. All chemical shifts were reported in ppm relative to the reference. Mass spectrum of the synthesized compound was recorded at Water Micromass-Q-T of Micro. The absorption spectra were recorded on SHIMADZU-2600 spectrophotometer using quartz cuvettes of 1 cm in path length. The fluorescence spectra were recorded on a Varian Carey Eclipse fluorescence spectrophotometer using a slit width (excitation = 20 nm, emission = 20 nm) at stated excitation. The stock solution of various cations and anions of concentration 1×10^{-1} molL^{-1} were prepared to form their corresponding perchlorate and tetra butyl ammonium salts, respectively. A stock solution of dyad **1** was prepared at 10^{-3} M (25mL) in DMSO/CH_3CN (10:15; v/v). The diluted solution was used further for photophysical studies in respective solvents. The stoichiometry of complexes was determined by Job`s Plot.

2.2. Calculation of binding constant

The binding constants of dyad **1** for different analytes were determined using the following Benesi-Hildebrand equation (1)

$$\frac{1}{I-I_0} = \frac{1}{K_a(I_{max}-I_0)[C]^n} + \frac{1}{I_{max}-I_0} \quad (1)$$

Where I_0, I, and I_{max} are the absorption/emission intensities of the dyad in absence of analyte, at an intermediate analyte concentration, and at a concentration of complete interaction with an analyte, respectively. K_a is the binding constant, C is the concentration of analyte, and n is the number of analytes bound per molecule.

2.3. Calculation of detection limit

The detection limit was calculated based on the fluorescence titration using IUPAC equation

Detection limit = 3σ/k

Where σ is the standard deviation of blank measurements [also defined as signal to noise (S/N) ratio], k is the slope of intensity versus sample concentration.

To determine the S/N ratio, the emission intensity of the dyad **1** (20 μM) was measured 3 times and the standard deviation of blank measurement was determined.

2.4. Quantum yield calculation

The fluorescence quantum yield ϕ_s for dyad **1** has been calculated in CH_3CN using following equation 2.

$$\Phi_S = \Phi_r \times \frac{1-10^{-A_r L_r}}{1-10^{-A_S L_S}} \times \frac{N_s^2}{N_r^2} \times \frac{D_s}{D_r} \quad (2)$$

Where, ϕ_s, As, L_s, N_s D_s represents the quantum yield, absorbance, length of absorption cell, refractive index and area under the emission for dyad 1, respectively. ϕ_r, A_r, L_r, N_r D_r represents the quantum yield, absorbance, length of absorption cell, refractive index and area under the emission for reference, respectively. The reference was used for calculation was rhodamine for similar optical response, (ϕ_r = 0.49, CH_3CH_2OH).

2.5. Computational Study

All the structural optimizations of the dyad and its complexes with Hg^{2+} and PPi were performed with Gaussian G03W[25] using Density Functional Theory (DFT) method. All the calculation were performed in the gas phase with hybrid functional B3LYP using basis sets 6-31G(d,p) for C, H, N, O, P and LANL2DZ for Hg^{2+}.

2.6. Synthesis of dyad 1

Synthesis of dyad **1** has been presented in scheme **1**. (4-(1*H*-phenanthro[9,10-*d*]imidazol-2-yl))benzaldehyde) (**4**) has been synthesized according to the reported procedure.[45,6] **S**olution of 1*H*-phenanthro[9,10-*d*]imidazol-2-yl)benzaldehyde **(4)** (1 g, 3.1 mmol)

DOI: 10.1039/C8NJ00741A

and 1,2-diaminoanthracen-9,10-dione (0.74 g, 3.1 mmol) in nitrobenzene (3 ml) was heated at 120 ˚C for 24 h. The reaction was monitored through TLC and after completion of the reaction, the reaction mixture was cooled to room temperature. The solid precipitate was separated out, filtered and washed with diethyl ether. The crude product was further purified by column chromatography. Yield = 57%; red solid; m.pt. = 235-237 ˚C; ^{1}H NMR ($CDCl_3$ + DMSO-d_6, 400 MHz): δ (ppm) 13.47 (s, 1H, NH), 13.10 (s, 1H, NH), 8.80-8.74 (m, 2H, ArH), 8.56-8.47 (m, 4H, ArH), 8.38 (d, 2H, *J* = 4 Hz, ArH), 8.20-7.99 (m, 4H, ArH), 7.89-7.79 (m, 2H, ArH), 7.69-7.57 (m, 4H, ArH); ^{13}C NMR ($CDCl_3$ + DMSO-d_6, 100 MHz): δ (ppm) 185.3, 181.1, 149.2, 142.9, 139.8, 134.9, 133.8, 132.7, 129.4, 128.7, 127.9, 126.8, 126.6, 126.3, 126.1, 125.2, 123.4, 122.8, 122.1, 120.2, 115.1, 112.1 (ArC); MS (ESI) m/z 541.0 (M^+ + H). Elemental Analysis. Mol. Formula $C_{36}H_{20}N_4O_2$, Calculated: C: 79.99, H: 3.73, N: 10.36. Found: C: 79.93, H: 3.68, N: 10.29.

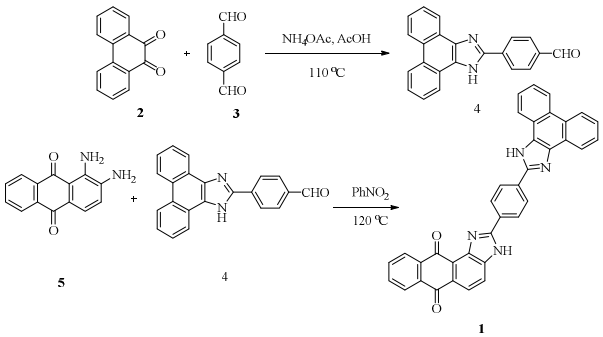

Scheme 1. Synthesis of dyad **1**

3. Results and discussion

3.1. Photophysical properties of dyad 1

The photophysical properties of dyad **1** were examined through absorption and emission spectroscopic techniques. The dyad **1** (20 µM, H_2O/CH_3CN (1:9; v/v), HEPES buffer (7.12 pH, 2 mM)) exhibited absorption peak at 430 nm, along with two shoulder peaks at 370 nm and 337 nm associated with yellow colour. However, on excitation at 430 nm, the dyad **1** exhibited the emission at 530 nm, accompanied by stokes shift of 100 nm (**Figure 1a**).

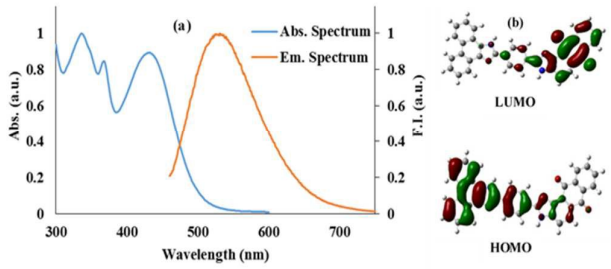

Figure 1. (a) Normalized absorption and emission spectra of dyad **1** (20 µM, H_2O/CH_3CN (1:9; V/V), HEPES buffer (7.12 pH, 2 mM) **(b)** frontier molecular orbitals for optimized structure of dyad **1**.

Dyad **1** contains 1*H*-phenanthro[9,10-*d*]imidazolequinone as an electron donor, anthraquinone unit as an electron acceptor and both linked through phenyl ring, thus presenting a D-π-A molecular system. The large stokes' shift and presence of donor-acceptor system suggested the charge transfer phenomenon, which was further evaluated by DFT calculations. The molecular configuration of dyad **1** was optimized and frontier molecular orbitals (FMO) were analyzed. It has been observed that dyad **1** was optimized in π-conjugated planar structure. The HOMO of dyad **1** was distributed over the donor phenanthrenequinone and extended over linker phenyl ring, while the LUMO was found to be distributed over anthraquinone unit (**Figure 1b**). Thus, the HOMO to LUMO transition clearly depicted intramolecular charge transfer phenomenon for dyad **1**. Additionally, the absorption and emission spectra of dyad **1** were analyzed in different solvents and it has been found that there was a redshift of 20 nm in absorption spectra on increasing the polarity of the solvent. Dyad **1** extended its emission maxima region from 430 nm to 610 nm by increasing the polarity of the solvent, which clearly depicted the stabilization of excited state in polar solvents (**Figure 2**). Thus, an extension of the emission spectrum at high polarity could be due to the presence of charge transfer, as endorsed by DFT calculations.

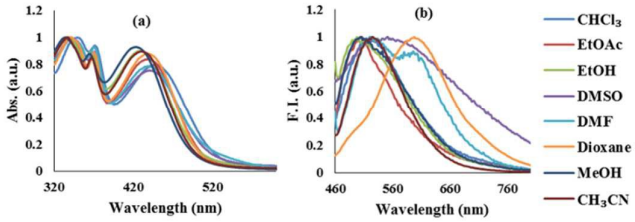

Figure 2. Normalized (a) absorption and (b) emission spectra of dyad **1** in presence of different solvents.

3.2. Sensing properties of dyad 1

The dyad **1** displayed yellow colour absorption maxima at 430 nm, and emission at 530 nm with stokes' shift of 100 nm in H_2O/CH_3CN (1:9; v/v). The recognition behavior of dyad **1** for different metal ions as their perchlorate salts *viz*., Na^+, K^+, Mg^{2+}, Ca^{2+}, Ba^{2+}, Cr^{3+}, Fe^{3+}, Co^{2+}, Ni^{2+}, Cu^{2+}, Zn^{2+}, Ag^+, Hg^{2+}, and Pb^{2+} and anions as their tetrabutylammonium salts *viz*., F^-, CN^-, Cl^-, SCN^-, AcO^-, NO_3^-, Br^-, HSO_4^-, $H_2PO_4^-$, I^-, and PPi have been examined. It has been found that amongst these metal ions and anions the dyad selectively detects the Hg^{2+} and PPi in H_2O/CH_3CN (1:9; v/v) through absorption and emission spectroscopic techniques.

3.2.1. Absorption behaviour of dyad 1 towards metal ions

The preliminary studies of the interaction of dyad 1 towards various metal ions as their perchlorate salts *viz*., Na^+, K^+, Mg^{2+}, Ca^{2+}, Ba^{2+}, Cr^{3+}, Fe^{3+}, Co^{2+}, Ni^{2+}, Cu^{2+}, Zn^{2+}, Ag^+, Hg^{2+}, and Pb^{2+} in H_2O/CH_3CN (1:9; v/v) solvent system. Dyad 1 showed no significant change in the absorption spectrum except in case of Hg^{2+} ions (**Figure 3a**).

View Article Online
DOI: 10.1039/C8NJ00741A

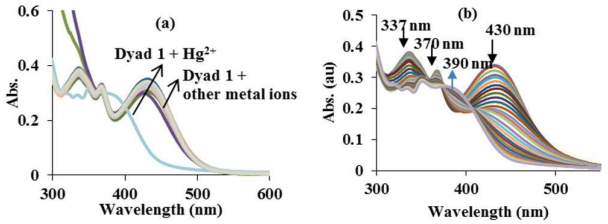

Figure 3. (a) Absorption response of dyad **1** (20 μM) towards different metal ions in H_2O/CH_3CN (1:9; v/v); **(b)** absorption response of dyad **1** (20 μM, H_2O/CH_3CN (1:9; V/V) , HEPES buffer (7.12 pH, 2 mM)) on increasing the concentration of Hg^{2+} ions.

Further, the incremental addition of Hg^{2+} (0 - 250 μM) to the solution of dyad **1**, the absorption intensity at 430, 370 and 337 nm decreased and concomitantly a new absorption band at 390 nm was formed (**Figure 3b**). The ratio of absorption intensities at 390 nm and 430 nm (A_{390}/A_{430}) exhibited a drastic change from 0.652 in the absence of Hg^{2+} ions to 3.083 in the presence of Hg^{2+} ions (2-240 μM) showing 5- fold variation in the absorption ratio.

3.2.2. Emission behaviour of dyad 1 towards various metal ions

The addition of various metal ions as their perchlorate salts *viz.*, Na^+, K^+, Mg^{2+}, Ca^{2+}, Ba^{2+}, Cr^{3+}, Fe^{3+}, Co^{2+}, Ni^{2+}, Cu^{2+}, Zn^{2+}, Ag^+, Hg^{2+}, and Pb^{2+} to dyad **1** in 20 μM, H_2O/CH_3CN (1:9; v/v), HEPES buffer (7.12 pH, 2 mM) solvent system showed fluorescence quenching, selectively on the addition of Hg^{2+} ions. Dyad **1** did not show any interaction with other metal ions significantly (**Figure 4a**). The gradual addition of Hg^{2+} ions to the solution of dyad **1,** decreased the emission intensity at 530 nm (**Figure 4b**). Further, this data has been utilized to calculate the binding constant using Benesi-Hildebrand equation and found to be 4×10^4 M^{-1} (**Figure S4a**). It has also been observed that dyad **1** showed a linear emission response for Hg^{2+} ions, as the lowest detection limit has been calculated to be 31 nM (**Figure S4b**).

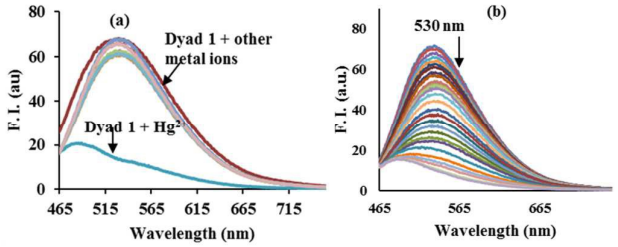

Figure 4. Fluorescence response of dyad **1** (20 μM, H_2O/CH_3CN (1:9; v/v) , HEPES buffer (7.12 pH, 2 mM)) (a) with different metal ions; **(b)** on increasing the concentration of Hg^{2+} ions.

3.2.3. Interference study of dyad 1 for Hg^{2+} ions

To determine the interference of other metal ions towards dyad **1** (20 μM, H_2O/CH_3CN (1:9; v/v) (20 μM, H_2O/CH_3CN (1:9; v/v), HEPES buffer (7.12 pH, 2 mM)), as Hg^{2+} sensor, competitive experiments were carried out. The emission response of dyad **1** was measured in the presence of 20 μM of Hg^{2+} and 1000 μM of other interfering metal ions such as Na^+, K^+, Mg^{2+}, Ca^{2+}, Ba^{2+}, Cr^{3+}, Fe^{3+}, Co^{2+}, Ni^{2+}, Cu^{2+}, Zn^{2+}, Ag^+ and Pb^{2+}. No significant interferences were observed in presence or absence of competitive metal ions (λ_{em} = 530 nm) as shown in **Figure 5**. Thus, dyad **1** could effectively detect the Hg^{2+} ions competitively in the presence of other metals ions.

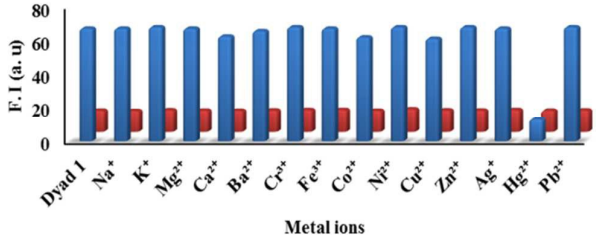

Figure 5. Blue bars represent the selectivity of dyad **1** (20 μM, H_2O/CH_3CN (1:9; V/V) , HEPES buffer (7.12 pH, 2 mM), λ_{em} = 530 nm) upon addition of different metal ions and red bars show the competitive selectivity of dyad **1** in the presence of Hg^{2+} ions.

3.2.4. Binding mode of dyad 1 with Hg^{2+}

To determine the stoichiometry of complex, a series of solutions containing dyad **1** and Hg^{2+} ions were prepared with variations of mole fractions (X) of Hg^{2+} from 0.1 to 1.0. The emission at 530 nm was plotted against the molar fraction of the Hg^{2+} solution. Based on Job plot, the complexation ratio of Hg^{2+} and dyad **1** has been found to be 1:1 (**Figure S5**).

3.2.5. Absorption behaviour of dyad 1 towards various anions

The presence of NH-groups in dyad **1** prompted us to evaluate its binding properties towards different anions of biological interest. On addition of anions *viz.*, F^-, CN^-, Cl^-, SCN^-, AcO^-, NO_3^-, Br^-, HSO_4^-, $H_2PO_4^-$, and I^- ions, no significant change in absorption was observed (**Figure 6a**). However, the addition of pyrophosphate ions (PPi) to the solution of dyad **1** showed a new red-shifted absorption band. Upon, gradual addition of PPi (0-60 μM) to the solution of dyad **1**, the absorption intensity at 430 nm decreased with concomitant increase in absorption intensity at 495 nm with an isosbestic point at 460 nm (**Figure 6b**). This ratiometric response of dyad **1** for PPi has been found to be 8-fold with the ratios of absorption intensities at 495 and 430 nm (A_{495}/A_{430}), exhibited a ratio change from 0.182 to 1.385 in the presence of 1-60 μM PPi. The spectral changes were accompanied with colour change form yellow to purple (**Figure S6**).

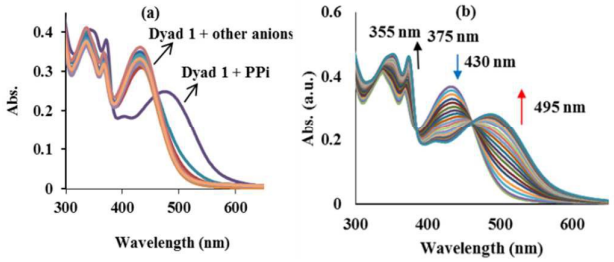

Figure 6. Absorption response of dyad 1 (20 μM, H2O/CH3CN (1:9; v/v) , HEPES buffer (7.12 pH, 2 mM)) (a) towards different anions; (b) on increasing the concentration of PPi.

View Article Online
DOI: 10.1039/C8NJ00741A

3.2.6. Emission behavior of dyad 1 towards various anions

Following the absorption results, the recognition behavior of dyad **1** towards anions has also been studied through fluorescence spectroscopy. It has been observed that the addition of anions *viz*., F^-, CN^-, Cl^-, SCN^-, AcO^-, NO_3^-, Br^-, HSO_4^-, $H_2PO_4^-$, I^-, ATP, and ADP ions have no variations in emission properties of dyad **1**. However, the introduction of PPi to the solution of dyad **1**, showed a red shift in emission band at 620 nm (**Figure 7a**). Upon, gradual addition of PPi to the solution of dyad **1**, the emission at 530 nm was quenched and a new emission band at 620 nm emerged that achieved its plateau after addition of 80 μM PPi with an isoemissive point at 560 nm (**Figure 7b**). In addition, the quantum yield of dyad **1** has been determined to be 0.1, while the presence of PPi in dyad **1** showed an increase in quantum yield to 0.69. Thus, the ratiometric response of dyad **1** towards PPi showed 60-folds variation in emission with a ratio of emission intensities at 620 and 530 nm (I_{620}/I_{530}), exhibiting a change from 0.263 to 15.917. The binding constant of dyad **1** towards PPi was calculated to be 1.7×10^4 M^{-1} (**Figure S7a**). It has been observed that dyad **1** showed a linear emission response for PPi and the lowest detection limit was calculated to be 46.5 nM (**Figure S7b)**.

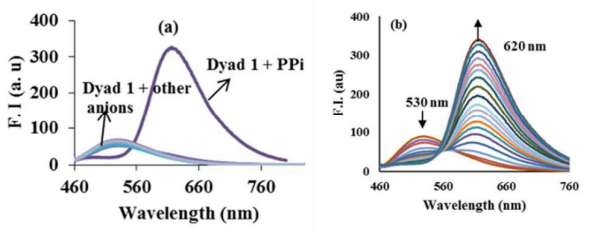

Figure 7. Fluorescence response of dyad **1** (20 μM, H_2O/CH_3CN (1:9; v/v) , HEPES buffer (7.12 pH, 2 mM)) **(a)** in the presence of different anions; **(b)** on gradual addition of PPi.

3.2.7. Interference study of dyad 1 for PPi

To determine the interference of other anions towards PPi for dyad **1**, competitive experiments were carried out in the presence of 100 μM of PPi mixed with 1000 μM of each of the different ions *viz*. F^-, CN^-, Cl^-, SCN^-, AcO^-, NO_3^-, Br^-, HSO_4^-, $H_2PO_4^-$, I^-, ATP, and ADP ions. No significant variation in the fluorescence intensity was observed in the presence of anions (λ_{em} = 620 nm) (**Figure 8**). Thus, dyad **1** showed higher sensitivity as well as the faster response among examined anions.

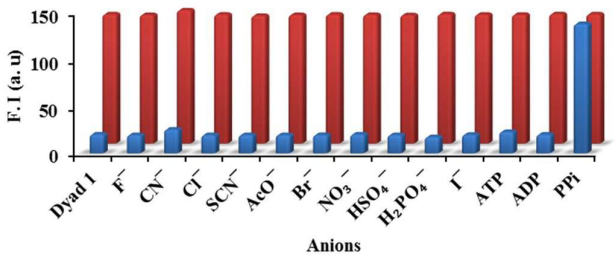

Figure 8. Blue bars represent the selectivity of dyad **1** (20 μM, H_2O/CH_3CN (1:9; V/V) , HEPES buffer (7.12 pH, 2 mM), at λ_{em} = 620 nm upon addition of different anions and red bars show the competitive selectivity of dyad 1 in the presence of PPi.

3.3. Computational study

In order to confirm the binding mode of dyad 1 towards Hg^{2+} ions and PPi , the structural optimizations for all molecules were carried out at DFT/B3LYP level of theories using 6-31G** basis sets for C, H, N, O, P and LANL2DZ for the Hg^{2+} ion. In addition, absorption properties were analysed by vertical Frank Condon excitation energy calculation using the time-dependent density functional theory (TD-DFT) method.

The dyad **1** comprises of phenanthroline and anthraquinone moieties linked through phenyl ring via a single bond, which increases the rotational flexibility. Therefore, to find local minima for dyad **1**, potential energy surface for dihedral angle between phenyl and anthraquinone moieties was performed at B3LYP/6-31G* level of theory. It has been found that the potential energy surface (PES) has two minima, assigned as **Form I** and **Form II**, where **Form I** was stabilized by 3.7 kcal mol^{-1} relative to **Form II** (Figure 9). Therefore, **Form I** was selected for further calculation and it was optimized at B3LYP/6-31++G** level of theory. The dyad **1** was found to be in a planar π-conjugated structure in the ground state, where the imidazole protons (NH) on phenanthraquinone and anthraquinone were present at *trans*-configuration to each other. The imidazole N–H bond distances were found to be 1.01 Å for dyad **1**.

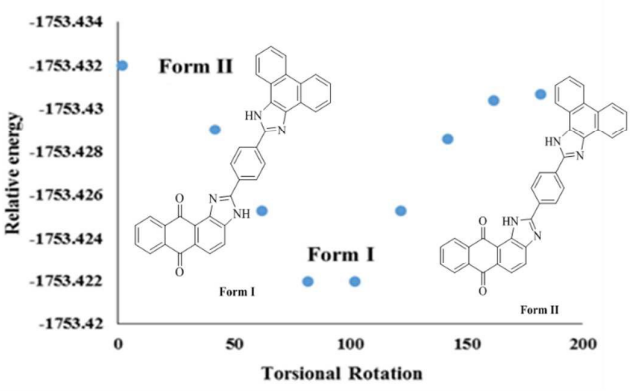

Figure 9. The relative energy changes for torsional rotation for dyad 1 from Form I to Form II.

Further, the structural optimization of complex dyad **1**.Hg^{2+} leads to coordination through quinone oxygen and imidazole nitrogen atoms. The interacting distances for O–Hg and N–Hg were found to be 2.38 Å and 2.40 Å, respectively, which were less than sum of vander Waal radii of nitrogen, oxygen and mercury [r_v(N) = 1.52 Å, r_v(O) = 1.52 Å, r_v(Hg) = 1.55 Å]. The predicted charges at oxygen and nitrogen atoms were found to be -0.374 and -0.274, which clearly predicted the dipolar interaction with Hg atom with charge of 0.676 units and support the coordination. Further, the absorption transitions, oscillation strength, and molecular orbital contribution of dyad **1**, and dyad **1**.Hg^{2+} were calculated and results are presented in **Table 1** and **Figure 10**. The frontier molecular orbital analysis of dyad 1 showed that the HOMO to LUMO, the electron density on donor phenanthro-benzimidazole and

View Article Online
DOI: 10.1039/C8NJ00741A

phenyl linker, decreased distinctly, while the acceptor anthraquinone-benzimidazole electron density has increased significantly. This clearly indicates the intramolecular charge transfer from donor phenanthro-benzimidazole to anthraquinone-benzimidazole *via* D-π-A transition. On the other hand, the predicted vertical Frank Condon transition for complex dyad **1**.Hg^{2+} ions at 442 nm has been found to be due o transition from phenanthro[9,10-*d*]imidazole to linker phenyl ring. Thus, the charge transfer from donor to acceptor has been restricted and utilized for coordination to Hg2+ metal.

Table 1: The calculated absorption value for dyad **1** in gas state, symmetry of frontier orbital and % contributions of molecular orbitals

λ_{Gas} (nm)	λ_{Exp} (nm)	Osc. Strength	Symmetry	% Orbital Contribution	
Dyad 1					
500.58	430	0.4075	Singlet-A	H→L	99
Dyad 1.Hg^{2+}					
442.74	390	0.6473	Singlet-A	H→L+2	90

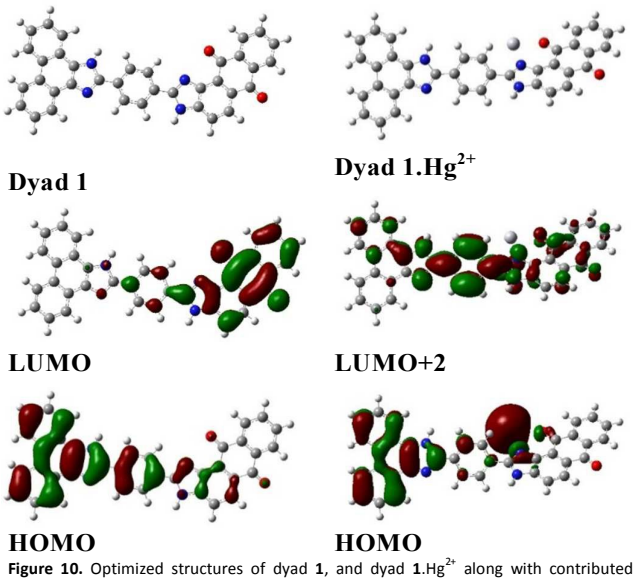

Figure 10. Optimized structures of dyad **1**, and dyad **1**.Hg^{2+} along with contributed frontier molecular orbitals for the transition.

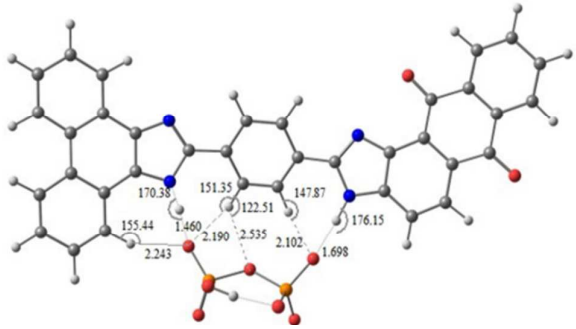

Figure 11. The optimized structure of dyad **1**.PPi adduct

On the other hand, the structural optimization of dyad **1.**PPi has been carried at the same level of theory. The optimized structure showed that the dyad **1** interacted with PPi through hydrogen bonding.[27] It has been found that the dyad **1** flipped from **Form I** to **Form II** such that oxygen atoms of PPi interacted to hydrogen atoms of NH of imidazole units of dyad **1**. The dyad **1**.PPi found to be stabilized in planar in geometry pertaining no alteration to conjugation. The interacting distances between N–H···O were found to be 1.46 Å and 1.70 Å, which were less than van der Waal's radii of hydrogen and oxygen atoms. The zero alteration in conjugation resulted in strong intramolecular charge transfer from electron donor phenanthroline to electron acceptor anthraquinone and PPi moieties (**Figure 11**).

Further, the existence of hydrogen bonding was examined based on Popelier criteria by means of the Bader's quantum theory of atoms in molecules (QTAIM) using multiwfn 3.3.8. These criteria are (i) occurrence of critical point (CP) between two neighboring atoms, (ii) the electron density [$\rho(r_c)$] must be in range of 0.002-0.034 au and (iii) the laplacian of electron density [$\nabla^2\rho(r_c)$] must be in range of 0.024-0.139 au at critical point. The positive value of Laplacian of electron density [$\nabla^2\rho(r_c)$] for all interactions, depicted electrostatic close shell interaction and the value found to be within Popelier's hydrogen bonding criteria. Further, the interactions were found to be medium range hydrogen bonds with partial covalent character except for NH…O (anthraquinone-imidazole) and ArH…O (bridged oxygen of PPi), which were weak in nature having electrostatic nature according to Rozas' rules. Moreover, the hydrogen bond energy is determined by Espinosa equation,[4646] which states that the interaction energy of H···X contact is defined as, E_{HX} = V(r)/2 at BCP, where V(r) is potential electron density at a bond critical point. The dyad **1**.PPi manifested by interactions NH···O and ArH···N, contributed -50.91 kcal mol^{-1} stabilization. The bond critical points and bond paths for both forms have been shown in **Figure S8.** The topological parameters were summarized in **Table 3**. It has been observed that the NH···O hydrogen bonds are of medium range with partial covalent character, while the ArH···O interaction were weak in nature with electrostatic character.

4. Determination of Hg^{2+} in water samples- To examine the sensitivity and analytical performance, conceptual experiment for dyad **1** was conducted. One sample was collected from pond near to industrial area Patiala, while second sample was taken as municipal tap water connection. Both samples were filtered through 0.6 μm membrane. The Filtered samples were then spiked with 3 ppm of Hg^{2+} ions. Further, the estimation of Hg^{2+} ion were carried through Atomic Absorption Spectroscopy (AAS analysis) and Fluorescence response. The analysis were carried out triplicated and the observed level of Hg^{2+} ions through AAS and emission spectra were summarized in Table 2. The averaged outputs of level of Hg^{2+} ion revealed similar results through both techniques, thus, the dyad **1** could be used to determination of Hg^{2+} ions in ground water.

Table 2. Determination of Hg^{2+} in water samples.

View Article Online
DOI: 10.1039/C8NJ00741A

Sample	Amount of Hg^{2+} detected by AAS in ppm after spiking	Amount of Hg^{2+} detected by fluorescence in ppm
Tap Water 1	2.76	2.706
Pond Water 2	1.367	1.315

In addition to this, the reversibility nature of dyad **1** was examined for Hg^{2+} ions and PPi ions. It has been observed that emission of dyad **1** decreases at 530 nm in presence of Hg^{2+} ions and PPi. However, the emission at 620 nm enhanced in presence of PPi, which did not alter significantly in presence of Hg^{2+} ions. On the other hand, the decreased emission of dyad 1 in presence of Hg2+ ion, showed enhancement on addition of PPi at 620 nm. Thus, the presence of PPi to dyad **1** and dyad **1**.Hg^{2+} showed a turn on emission at 620 nm.

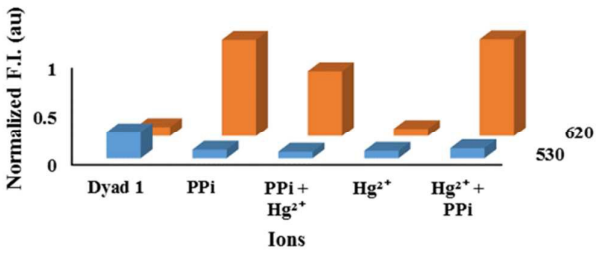

Figure 12. Change in emission on addition of Hg2+ ions and PPi to Dyad 1

5. Conclusions

In summary, a pretentious donor-π-acceptor (D-π-A) dyad was synthesized and successfully utilized in detection of Hg^{2+} and PPi in semi-aqueous medium. The D-π-A molecular system has been constructed by linking phenanthraquinone for an electron donor unit and anthraquinone for an electron acceptor unit through a phenyl ring. Dyad **1** exhibited the intramolecular charge transfer, and acts as key phenomenon for detection of Hg^{2+} and PPi. The dyad **1** showed the absorption and emission quenching in presence of Hg^{2+} ions. The DFT calculation endorsed the experimental results. The frontier molecular orbital analysis clearly depicted the charge transfer from donor to acceptor for dyad **1**, which has been restricted on complexation with Hg^{2+}. On the other hand, the presence of PPi resulted in drastic changes in absorption and emission spectra of dyad **1**. The dyad **1**.PPi has been stabilized through NH···O and ArH···O hydrogen bonding and analyzed through AIM calculation. The NH···O interactions were found to be medium range with partial covalent character and ArH···O interaction were weak with electrostatic in nature. The quantum yield of dyad **1** on complexation with PPi was also increased to from 0.1 to 0.69.

Table 3. Topological parameters Laplacian electron density ($\nabla^2\rho$), potential energy density [V(r)], Lagrangian kinetic energy G(r), total energy density [H(r)], hydrogen bonding energy [E_{HB}($kJmol^{-1}$)] at a bond critical pint of non-covalent interactions (D···HA) for dyad **1**.PPi adduct at B3LYP/6-31G**.

Interactions	BCP	d(Å)	∠D···HA	$\nabla^2\rho$	V(r)	G(r)	H(r)	E_{HB}
NH···O	(3,-1)	1.46	170.38	0.1547	-0.0812	0.0599	-0.0213	-25.58
ArH···O	(3,-1)	2.19	151.35	0.0517	-0.0142	0.0136	-0.0006	-4.47
ArH···O	(3,-1)	2.10	147.87	0.0595	-0.0172	0.0161	-0.0012	-5.42
ArH···O	(3,-1)	2.24	155.40	0.0420	-0.0117	0.0111	-0.0006	-3.69
NH···O	(3,-1)	1.70	176.15	0.1278	-0.0308	0.0314	0.0005	-9.70
ArH···O	(3,-1)	2.54	122.51	0.0344	-0.0065	0.0075	0.0011	-2.05

Conflicts of interest

Authors declare no conflicts of interest.

Acknowledgements

We thank DST-INSPIRE (IFA12-CH-59), New Delhi for fellowship and financial assistance. We are also thankful to SAI Labs, Thapar University, Patiala and SAIF (Panjab University, Chandigarh) for NMR and Mass analysis.

Notes and references

1. L. You, D. Zha and E. V. Anslyn, *Chem Rev*, 2015, **115**, 7840-7892.
2. H. Zhu, J. Fan, B. Wang and X. Peng, *Chem. Soc. Rev.*, 2015, **44**, 4337-4366.
3. Y. Yang, Q. Zhao, W. Feng and F. Li, *Chem Rev*, 2013, **113**, 192-270.
4. S. Sasaki, G. P. Drummen and G.-i. Konishi, *J. Mater. Chem. C*, 2016, **4**, 2731-2743.
5. B. D. Wagner, *Phys. Chem. Chem. Phys.*, 2012, **14**, 8825-8835.
6. J. Wu, W. Liu, J. Ge, H. Zhang and P. Wang, *Chem. Soc. Rev.*, 2011, **40**, 3483-3495.
7. M. H. Lee, J. S. Kim and J. L. Sessler, *Chem. Soc. Rev.*, 2015, **44**, 4185-4191.
8. J. Zhao, S. Ji, Y. Chen, H. Guo and P. Yang, *Phys. Chem. Chem. Phys.*, 2012, **14**, 8803-8817.
9. X. Ma, L. Yan, X. Wang, Q. Guo and A. Xia, *Phys. Chem. Chem. Phys.*, 2011, **13**, 17273-17283.
10. Y. Olivier, M. Moral, L. Muccioli and J.-C. Sancho-García, *J. Mater. Chem. C*, 2017, **5**, 5718-5729.
11. H. Meier, Z.-S. Huang and D. Cao, *J. Mater. Chem. C*, 2017, **5**, 9828-9837.
12. A. M. Shaikh, S. Chacko and R. M. Kamble, *ChemistrySelect*, 2017, **2**, 7620-7629.
13. S. Yoon, E. W. Miller, Q. He, P. H. Do and C. J. Chang, *Angew. Chem., Int. Ed.*, 2007, **46**, 6658-6661.

View Article Online
DOI: 10.1039/C8NJ00741A

14. S.-Y. Ding, M. Dong, Y.-W. Wang, Y.-T. Chen, H.-Z. Wang, C.-Y. Su and W. Wang, *J. Am. Chem. Soc.*, 2016, **138**, 3031-3037.
15. E. M. Nolan and S. J. Lippard, *J. Am. Chem. Soc.*, 2007, **129**, 5910-5918.
16. X. Zhang, Y. Xiao and X. Qian, *Angew. Chem., Int. Ed.*, 2008, **47**, 8025-8029.
17. H. N. Kim, W. X. Ren, J. S. Kim and J. Yoon, *Chem. Soc. Rev.*, 2012, **41**, 3210-3244.
18. L. Zong, Y. Xie, Q. Li and Z. Li, *Sens. Actuators, B*, 2017, **238**, 735-743.
19. C. Wu, J. Wang, J. Shen, C. Bi and H. Zhou, *Sens. Actuators, B*, 2017, **243**, 678-683.
20. S. Zhang, S. Sun, M. Zhou, L. Wang and B. Zhang, *Sci Rep*, 2017, **7**, 43419.
21. J. Kandhadi, V. Yeduru, P. R. Bangal and L. Giribabu, *Phys. Chem. Chem. Phys.*, 2015, **17**, 26607-26620.
22. Y. Li, T. Tan, S. Wang, Y. Xiao and X. Li, *Dyes Pigm.*, 2017, **144**, 262-270.
23. N. Kaur and S. Kumar, *Dalton Trans.*, 2012, **41**, 5217-5224.
24. A. Sarkar, S. Bhattacharyya and A. Mukherjee, *Dalton Trans.*, 2016, **45**, 1166-1175.
25. J. Hu, Z. Hu, S. Liu, Q. Zhang, H.-W. Gao and K. Uvdal, *Sens. Actuators, B*, 2016, **230**, 639-644.
26. P. M. Reddy, S.-R. Hsieh, C.-J. Chang and J.-Y. Kang, *J. Hazard. Mater.*, 2017, **334**, 93-103.
27. A. Steinegger, I. Klimant and S. M. Borisov, *Advanced Optical Materials*, 2017, **5**.
28. L. Hou, X. Kong, Y. Wang, J. Chao, C. Li, C. Dong, Y. Wang and S. Shuang, *Journal of Materials Chemistry B*, 2017, **5**, 8957-8966.
29. Z. Li, W. Zhang, C. Liu, M. Yu, H. Zhang, L. Guo and L. Wei, *Sens. Actuators, B*, 2017, **241**, 665-671.
30. Y. Zhao, H. Li, Y. Xue, Y. Ren and T. Han, *Sens. Actuators, B*, 2017, **241**, 335-341.
31. D. Chao and S. Ni, *Sci. Rep.*, 2016, **6**, 26477.
32. V. D. Singh, R. S. Singh, R. P. Paitandi, B. K. Dwivedi, B. Maiti and D. S. Pandey, *The Journal of Physical Chemistry C*, 2018, **122**, 5178-5187.
33. K. A. Jolliffe, *Acc. Chem. Res.*, 2017, **50**, 2254-2263.
34. W. Wang, J. Wu, Q. Liu, Y. Gao, H. Liu and B. Zhao, *Tetrahedron Lett.*, 2018, **59**, 1860-1865.
35. Q. Wang, X. Wen and Z. Fan, *J. Photochem. Photobiol., A*, 2018, **358**, 92-99.
36. J. B. Chae, H. J. Jang and C. Kim, *Photochem. Photobiol. Sci.*, 2017, **16**, 1812-1820.
37. J. H. Kang, J. Han, H. Lee, M. H. Lim, K.-T. Kim and C. Kim, *Dyes Pigm.*, 2018, **152**, 131-138.
38. V. Luxami, K. Paul and I. H. Jeong, *Dalton Trans.*, 2013, **42**, 3783-3786.
39. S. M. Hwang, M. S. Kim, M. Lee, M. H. Lim and C. Kim, *New J. Chem.*, 2017, **41**, 15590-15600.
40. A. K. Purohit, B. N. Ghosh and P. K. Kar, *Spectrochim. Acta, Part A*, 2018, **188**, 547-550.
41. R. Goel, V. Luxami and K. Paul, *J. Photochem. Photobiol., A*, 2017, **348**, 102-109.
42. B. M. Long, F. M. Pfeffer and C. J. Barrow, *Sens. Actuators, B*, 2017, **243**, 761-764.
43. T. G. Jo, K. H. Bok, J. Han, M. H. Lim and C. Kim, *Dyes Pigm.*, 2017, **139**, 136-147.
44. Z.-X. Wang, X.-H. Yu, F. Li, F.-Y. Kong, W.-X. Lv and W. Wang, *Journal of Materials Chemistry B*, 2018, **6**, 1771-1781.
45. W. Lin, L. Long, L. Yuan, Z. Cao, B. Chen and W. Tan, *Org. Lett.*, 2008, **10**, 5577-5580.
46. E. Espinosa, E. Molins and C. Lecomte, *Chem. Phys. Lett.*, 1998, **285**, 170-173.

View Article Online
DOI: 10.1039/C8NJ00741A

Donor-π-Acceptor (D-π-A) Dyad for ratiometric detection of Hg^{2+} and PPi

Richa Rani†, Gulshan Kumar†, Kamaldeep Paul and Vijay Luxami*

School of Chemistry and Biochemistry, Thapar University, Patiala – 147 004, India.

Email: vluxami@thapar.edu